



# A High-Entropy B2 Heusler Alloy

Aslı Çakır<sup>1</sup> · Mehmet Acet<sup>2</sup> · Michael Farle<sup>2</sup>

Received: 25 August 2022 / Accepted: 27 January 2023 / Published online: 17 February 2023  
© The Author(s) 2023

## Abstract

The properties of high-entropy alloys containing five or more elements show systematic evolutions with varying valence-electron concentration. This can allow them to be tailored to carry a particular feature or a property. We have prepared a six-component alloy  $(\text{MnFeCoNiCu})_{75}\text{Al}_{25}$ , where MnFeCoNiCu makes up the high-entropy part with  $e/a = 9.0$  and the added 25 at.% Al causes the whole of the material to take up a B2-ordered structure with  $e/a = 7.5$ . Because the structure becomes ordered, the material partially loses its high-entropy character but acquires a ferromagnetic Heusler-like property with a Curie temperature of 525 K and an average magnetic moment of  $0.8 \mu_B$ . The whole of the system mimics  $\text{Co}_3\text{Al}$ , which cannot be stabilized under normal conditions.

**Keywords** High-entropy alloy · Heusler · Magnetic properties · Ferromagnetism

## Introduction

The magnetic properties of  $3d$  alloys and compounds are governed by the number of  $s$ - and  $d$ -valence electrons per atom,  $e/a$ , they carry and, to a large extent, also their structural properties [1]. This rule based on band magnetism also applies for multi-element alloys as well as high-entropy alloys and allows to predict their magnetic properties through the Slater–Pauling rule and the variation of the crystal structure along the transition-element series of the periodic table. The validity of the  $e/a$ -rule is mainly limited to the combination of the elements through the  $3d$  series. To a certain extent, they also apply for interstitial alloys and compounds of  $3d$  elements with B, C, and N and for alloys incorporating group 13–15 elements forming Heusler-type alloys [2, 3].

$3d$  high-entropy alloys make up no exceptions to this rule. The equiatomic Cantor alloy CrMnFeCoNi [4, 5] has  $e/a = 8$ , which is also the value for Fe. The difference is that the Cantor alloy is FCC at room temperature so that

from the electronic aspect, the Cantor alloy is equivalent to FCC-Fe [6–8]. Indeed, we had shown that the Cantor alloy possesses the predicted room-temperature properties of anti-Invar FCC-Fe. Based on this observation, one can predict that also Invar properties can be made to emerge in non-equiatomic, multi-component  $3d$  alloys by adjusting  $e/a$  to a value around 8.7. Such a multi-component alloy did indeed show features related to Invar properties in the thermal expansion, magnetization, and elastic modulus [9].

In this work, we prepare a multi-component compound based on the high-entropy alloy MnFeCoNiCu. We add Al to this alloy so that the end composition is tailored to be a  $(\text{MnFeCoNiCu})_3\text{Al}$ -ordered compound. MnFeCoNiCu has  $e/a = 9$ , namely equivalent to Co. In this manner, we expect to stabilize a pseudo- $\text{Co}_3\text{Al}$  compound with  $e/a = 7.5$  which under normal conditions cannot be stabilized. The substitution of one of the elements in a  $3d$  high-entropy alloy by Al tends to form mixed FCC–BCC phases with the BCC phase exhibiting B2 ordering in some cases [10–14]. We prepare and examine here the structural and in particular the magnetic properties of the ordered B2  $(\text{MnFeCoNiCu})_3\text{Al}$  compound expecting a magnetic moment of about  $0.8 \mu_B$  from the Slater–Pauling rule.

✉ Mehmet Acet  
mehmet.acet@uni-due.de

<sup>1</sup> Department of Metallurgical and Materials Engineering,  
Muğla Sıtkı Koçman University, 48000 Muğla, Turkey

<sup>2</sup> Faculty of Physics and Center for Nanointegration  
(CENIDE), Universität Duisburg-Essen, 47048 Duisburg,  
Germany

## Experimental

We prepared polycrystalline  $(\text{MnFeCoNiCu})_{75}\text{Al}_{25}$  by arc melting Mn, Fe, Co, Ni, Cu, and Al of 99.95% purity under Ar atmosphere in a water-cooled Cu crucible. We carried out a further homogenization for 5 days at 1273 K and quenched the sample in water at room temperature. The chemical compositions and homogeneities of the samples were determined by energy-dispersive X-ray analysis (EDX) using a scanning electron microscope (SEM). We determined the actual composition of the sample to be  $\text{Mn}_{14.1}\text{Fe}_{15.3}\text{Co}_{15.0}\text{Ni}_{14.9}\text{Cu}_{14.9}\text{Al}_{25.9}$ .

We carried out X-ray diffraction (XRD) measurements at room temperature using Cu K-alpha radiation. The results were refined using Le Bail fitting with Jana2006 software [15]. Magnetization measurements were carried out in a superconducting quantum interference device (SQUID) magnetometer in the temperature range  $10 \leq T \leq 750$  K.

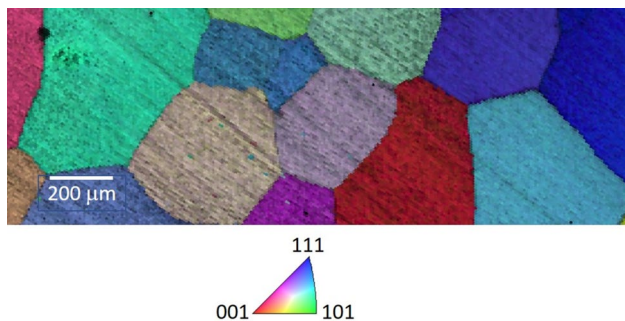


**Fig. 1** The microstructure of the sample. The orientation of the grains is given with the color scale (Color figure online)

## Results

The microstructure of the sample is shown in Fig. 1. The circle-diameter equivalent size of the grains is about 300–500  $\mu\text{m}$ . As will be presented below, the crystallographic structure is BCC/B2. The equiatomic high-entropy alloy MnFeCoNiCu is FCC [16]. Al stabilizes the BCC/B2 phase.

We show the results of EDX mapping in Fig. 2. The investigated area is shown in Fig. 2a along with the 116  $\mu\text{m}$  line-scan length. The results of the line-scan are given in Fig. 2b showing that the elements are homogeneously distributed. The homogeneity is also seen in the even distribution of all elements in Fig. 2c–h.

We give the results of the XRD measurements in Fig. 3. The sample used is a polished bulk specimen since obtaining a powder from the ductile specimen is not readily possible. The refinement was carried out using the  $Pm\bar{3}m$  space group. The structure is BCC with the emergence of the superstructure peaks (100), (111), and (210) evidencing the presence of the B2 phase. The lattice parameter  $a$  is estimated to be 0.2900 nm.

We show the temperature dependence of the magnetization  $M(T)$  in Fig. 4. Figure 4a and b shows the data obtained under 5 mT and 2 T, respectively, using zero-field-cooled (ZFC) and field-cooled (FC) protocols for  $10 \leq T \leq 300$  K. Before the measurement, the sample was demagnetized at 300 K and cooled to 10 K in zero field. 5 mT was then applied, and the data were taken on increasing temperature up to 300 K. The FC measurement was then continued by obtaining data on decreasing temperature. No splitting between data obtained under ZFC and FC conditions is

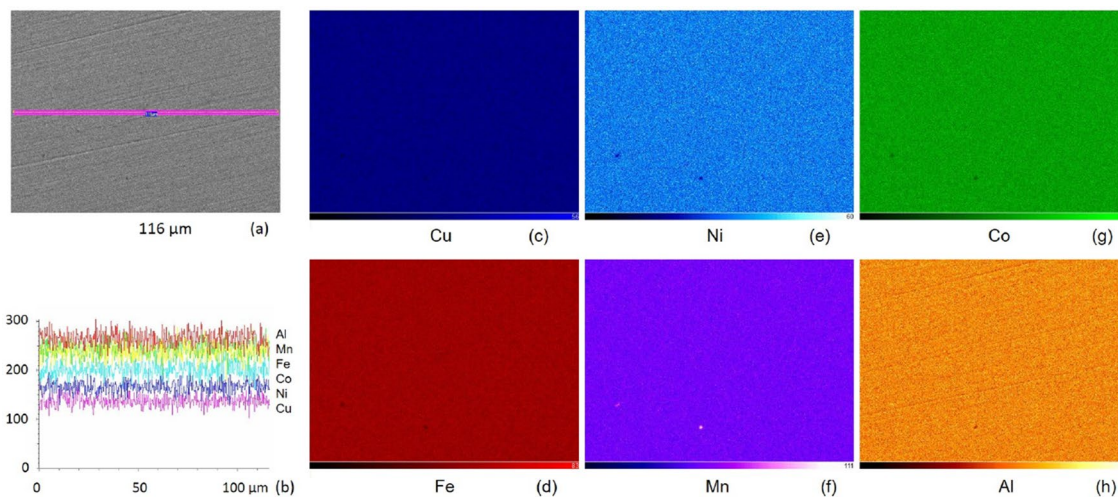


**Fig. 2** EDX mapping. **a** The general area ranging over 166  $\mu\text{m}$  and **b** the line scan over the region in **a** in pink. Elemental mapping of **c** Cu, **d** Fe, **e** Ni, **f** Mn, **g** Co, and **h** Al. The elements are uniformly distributed (Color figure online)

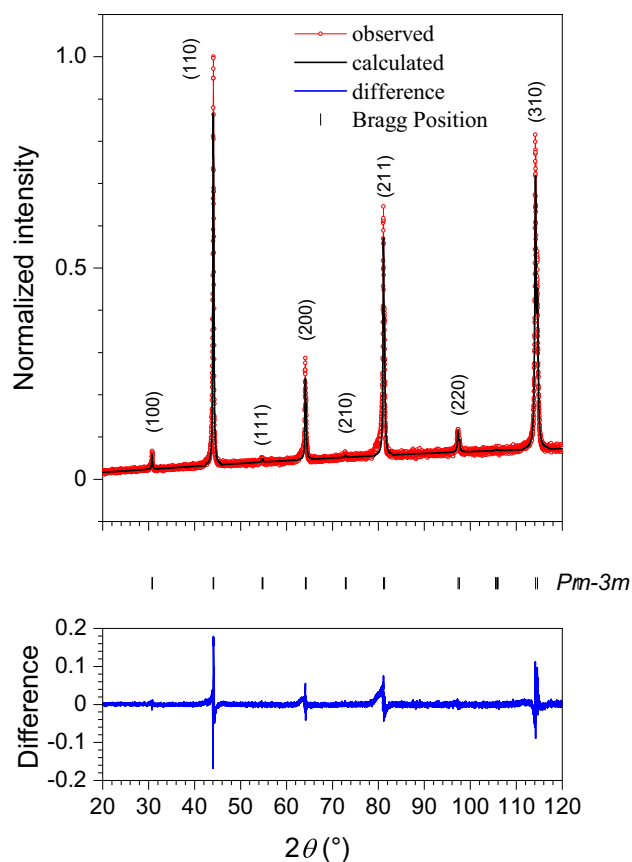


**Fig. 3** Refined XRD showing observed, calculated, and difference spectra. (100), (111), and (210) are B2 superstructure peaks

observed indicating the absence of any mixed antiferromagnetic/ferromagnetic interactions. The sample was then placed in a high-temperature oven accommodated in the SQUID, and the measurements were carried out only on increasing temperature. We estimate the Curie temperature  $T_C$  as 525 K. Whereas  $M(T)$  measured in small fields provides the determination of  $T_C$  with good precision,  $M(T)$  measured in fields corresponding to saturation provides the temperature behavior of the saturation magnetization. In this case, the magnetization obtained under 2 T corresponds to the saturation magnetization and conforms to a mean-field Brillouin behavior.

To understand if any post-annealing thermal treatments have an effect on the magnetic properties, we have carried out a sequential annealing  $M(T)$  run with a temperature-change protocol 300 → 500 → 400 → 600 → 400 → 650 → 400 → 700 → 400 → 750 K. The results are shown in Fig. 5. Figure 5a shows the data in the full temperature range, and Fig. 5b shows the same data in the vicinity of  $T_C$ . The measurements were carried out at a rate of 4 K min<sup>-1</sup>.  $T_C$  shows an increase each time the temperature is brought up above 600 K. When the temperature is decreased from each maximum temperature of a

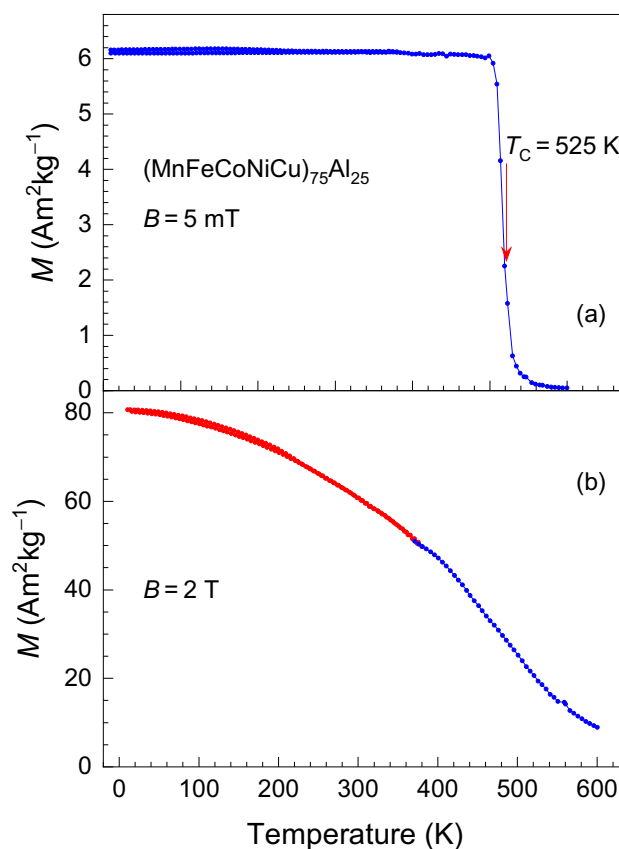


**Fig. 4**  $M(T)$  obtained over the temperature range  $10 \leq T \leq 600$  K under **a** 5 mT and **b** 2 T. Vertical arrow in **a** denotes  $T_C$

given run, the data retrace their path.  $T_C$  increases from 525 K to about 570 K within the time and temperature interval of the experiment.

We have measured  $M(B)$  at 10 K to reveal any feature that would be due to mixed magnetic interaction and to estimate the average magnetic moment (Fig. 6). We find no substantial high-field susceptibility that would have been evidence for the presence of non-ferromagnetic components. This is in agreement with the absence of ZFC–FC splitting in  $M(T)$  at low temperatures. The coercivity is essentially zero. The saturation magnetization  $M_s = 81.5 \text{ A m}^2 \text{ kg}^{-1}$  corresponding to a magnetic moment value of  $0.8 \mu_B$  per atom. Our results show that  $T_C$  increases when the sample is sequentially annealed. This is likely to be an effect of the increase in the degree of B2 ordering as the sample is progressively annealed.

## Discussion

There have been attempts to stabilize the  $\text{Co}_3\text{Al}$  phase in the past, and much theoretical work had been carried out to predict the properties. It was also shown that rapid solidification could lead to a metallic glass state.

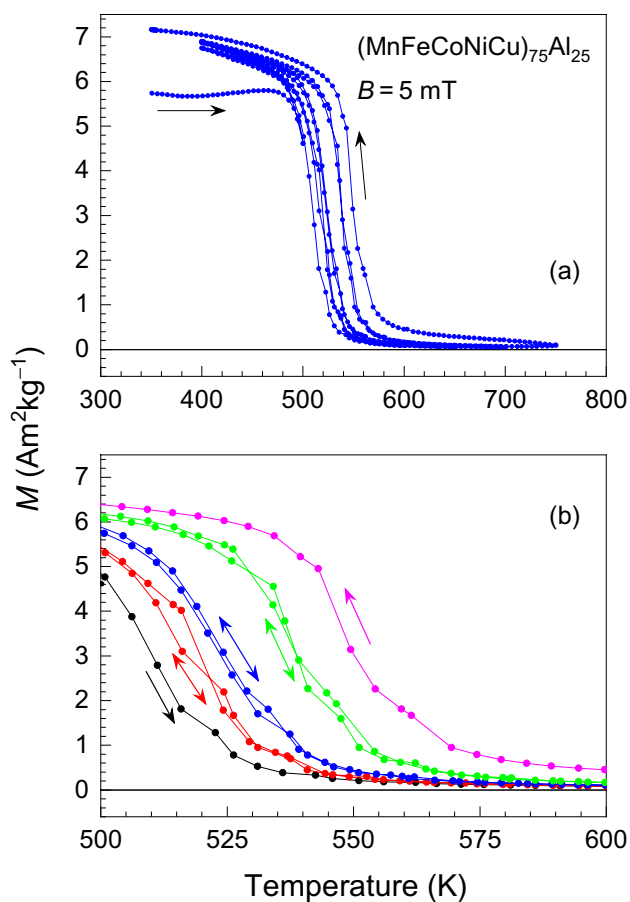


**Fig. 5**  $M(T)$  showing a sequential annealing measurement with a temperature protocol  $300 \rightarrow 500 \rightarrow 400 \rightarrow 600 \rightarrow 400 \rightarrow 650 \rightarrow 400 \rightarrow 700 \rightarrow 400 \rightarrow 750$  K. **a** Full temperature range, and **b** expanded plot for  $500 \leq T \leq 650$  K

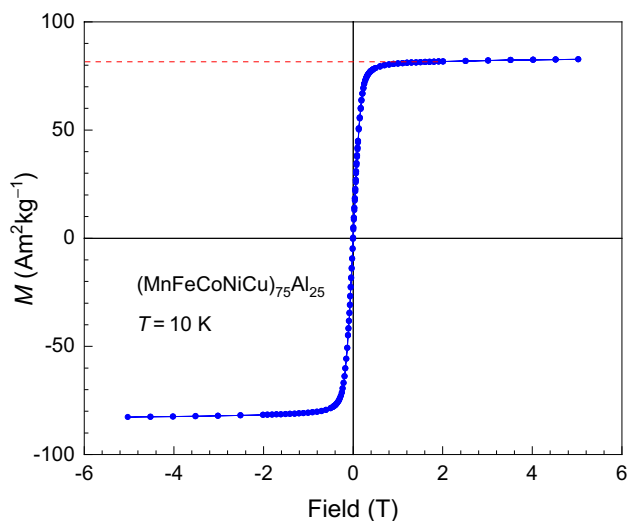


**Fig. 6**  $M(B)$  at 10 K. The dashed red line points to the value  $M_s = 81.5 \text{ A m}^2 \text{ kg}^{-1}$  corresponding to an  $e/a$ -value of  $0.8 \mu_B$  per atom (Color figure online)

High-entropy alloys are capable of acquiring crystallographic structures which do not occur in simple 3D metals with equivalent valence-electron concentrations. FCC-Fe is one example and  $\text{Co}_3\text{Al}$  is a second one with its electronic equivalent high-entropy alloy taken into hand in this work.  $(\text{MnFeCoNiCu})_3\text{Al}$  is purely ferromagnetic with  $e/a = 0.8 \mu_B$ . Low-field  $M(T)$  measurements show no indication of any mixed antiferromagnetic interactions. Their absence is also supported by the attainment of full saturation observed in  $M(B)$ .

The B2 ordering can only be compatible with the uniform distribution of the  $3d$  elements if Al takes up only body-centered position. The rest of the elements should then be randomly positioned so that the nearest neighbor atom to Al can be any one of the five  $3d$  species at random. In this manner, we have what could be regarded as a high-entropy B2 Heusler. The sequential annealing measurements show that full B2 ordering is yet to be achieved. This would depend on the time and temperature at which the annealing is carried out. The present results indicate that  $T_C$  increases as the temperature is cycled sequentially with the sample being exposed to elevated temperature for the time interval of the  $M(T)$  experiments taking place at  $4 \text{ K min}^{-1}$ . The degree of B2 ordering is known to affect  $T_C$  of B2 FeCo [17] so that a similar situation can be expected for the compound investigated in this work. Further neutron diffraction studies are needed to understand the degree of ordering and the stabilization conditions of the B2 phase.

## Conclusions

We have prepared a multi-component B2 compound starting with the high-entropy alloy MnFeCoNiCu and adding 25 at.% Al. The resulting compound  $(\text{MnFeCoNiCu})_3\text{Al}$  is B2 and ferromagnetic with  $T_C = 525$  K. The value of the magnetic moment  $0.8 \mu_B$  fits well to the Slater–Pauling scheme representing Heusler compounds. In this manner, we understand that unstable structures at certain  $e/a$ -values can be made to become stable by preparing their high-entropy alloy counterpart and adjusting the  $e/a$ -value.

**Acknowledgements** We would like to thank Jonas Ehrich and Robin Reimer for their assistance in optical and electron microscopy. We acknowledge the support of Deutsche Forschungsgemeinschaft (Project 405553726-CRC/TRR 270) and TUBITAK Science Fellowships and Grant Programs (Grant 1059B192000916).

**Author Contributions** The experiments were performed by AÇ and MA. The manuscript was prepared by the contribution of all authors.

**Funding** Open Access funding enabled and organized by Projekt DEAL.

**Data Availability** Data are available on request.

## Declarations

**Conflict of interest** The authors have no competing interests.

**Open Access** This article is licensed under a Creative Commons Attribution 4.0 International License, which permits use, sharing, adaptation, distribution and reproduction in any medium or format, as long as you give appropriate credit to the original author(s) and the source, provide a link to the Creative Commons licence, and indicate if changes were made. The images or other third party material in this article are included in the article's Creative Commons licence, unless indicated otherwise in a credit line to the material. If material is not included in the article's Creative Commons licence and your intended use is not permitted by statutory regulation or exceeds the permitted use, you will need to obtain permission directly from the copyright holder. To view a copy of this licence, visit <http://creativecommons.org/licenses/by/4.0/>.

## References

1. W. Pepperhoff, M. Acet, *Constitution and Magnetism of Iron and Its Alloys* Engineering Materials and Processes. (Springer, Berlin, 2001)
2. M. Acet, B. Gehrman, E.F. Wassermann, H. Bach, W. Pepperhoff, Relevance of magnetic instabilities to the properties of interstitial solid solutions and compounds of Fe. *J. Magn. Mater.* **232**, 221–230 (2001)
3. A. Çakır, L. Righi, F. Albertini, M. Acet, M. Farle, Intermartensitic transitions and phase stability in  $\text{Ni}_{50}\text{Mn}_{50-x}\text{Sn}_x$  Heusler alloys. *Acta Mater.* **99**, 140–149 (2015)
4. B. Cantor, I.T.H. Chang, P. Knight, A.J.B. Vincent, Microstructural development in equiatomic multicomponent alloys. *Mater. Sci. Eng. A* **375–377**, 213–218 (2014)
5. J.W. Yeh, S.K. Chen, S.J. Lin, J.Y. Gan, T.S. Chin, T.T. Shun, C.H. Tsau, S.Y. Chang, Nanostructured high-entropy alloys with multiple principal elements: novel alloy design concepts and outcomes. *Adv. Eng. Mater.* **6**, 299–303 (2004)
6. M. Acet, Inducing strong magnetism in  $\text{Cr}_{20}\text{Mn}_{20}\text{Fe}_{20}\text{Co}_{20}\text{Ni}_{20}$  high-entropy alloys by exploiting its anti-Invar property. *AIP Adv.* **9**, 095037 (2019)
7. O. Schneeweiss, M. Friák, M. Dudová, D. Holec, M. Sob, D. Kriegner, V. Holý, P. Beran, E.P. George, J. Neugebauer, A. Dlouhý, Magnetic properties of the CrMnFeCoNi high-entropy alloy. *Phys. Rev. B* **96**, 014437 (2017)
8. G. Laplanche, P. Gadaud, O. Horst, F. Otto, G. Eggeler, E.P. George, Temperature dependencies of the elastic moduli and thermal expansion coefficient of an equiatomic, single-phase CoCrFeMnNi high-entropy alloy. *J. Alloys Compd.* **623**, 348–353 (2015)
9. Z. Rao, A. Çakır, Ö. Özgün, D. Ponge, D. Raabe, Z. Li, M. Acet, Magnetic properties of the FCC- and  $\sigma$ -phases in equiatomic and off-equiatomic high-entropy Cantor alloys. *Phys. Rev. Mater.* **5**, 044406 (2021)
10. G.M. Muralikrishna, A.C.M. Esther, K. Guruvidyathri, P. Watermeyer, Ch.H. Liebscher, K.N. Kulkarni, G. Wilde, S.V. Divinski, B.S. Murty, Novel multicomponent B2-ordered aluminides: compositional design, synthesis, characterization, and thermal stability. *Metals* **10**, 1411 (2020)
11. C. Bazioti, O.M. Lovvik, A. Poulia, P.A. Carvalho, A.S. Azar, P. Mikheenko, S. Diplas, A.E. Gunaes, Probing the structural evolution and its impact on magnetic properties of  $\text{FeCoNi}(\text{AlMn})_x$  high-entropy alloy at the nanoscale. *J. Alloys Compd.* **910**, 164724 (2022)
12. J. Wang, P. Jiang, F. Yuan, X. Wu, Chemical medium-range order in a medium entropy alloy. *Nat. Commun.* **13**, 1021 (2022)
13. J. Wang, Z. Kou, S. Fu, S. Wu, S. Liu, M. Yan, Z. Ren, D. Wang, Z. You, S. Lan, H. Hahn, X.-L. Wang, T. Feng, Ultrahard BCC-AlCoCrFeNi bulk nanocrystalline high-entropy alloy formed by nanoscale diffusion-induced phase transition. *J. Mater. Sci. Technol.* **115**, 29–39 (2022)
14. W. Zhang, Z. Ma, C. Li, C. Guo, D. Liu, H. Zhao, L. Ren, Micro/nano-mechanical behaviors of individual FCC, BCC and FCC/BCC interphase in a high-entropy alloy. *J. Mater. Sci. Technol.* **114**, 102–110 (2022)
15. V. Petříček, M. Dušek, L. Palatinus, Crystallographic Computing System JANA2006: General features. *Z. Kristallogr.* **229**, 345–352 (2014)
16. T. Uddin, K. Biswas, N.P. Gurao, Deciphering micro-mechanisms of plastic deformation in a novel single phase fcc-based MnFeCoNiCu high entropy alloy using crystallographic texture. *Mater. Sci. Eng. A* **657**, 224–233 (2016)
17. J. Orehtsky, K. Schroder, Order-disorder critical phenomena in FeCo. *J. Phys. F* **4**, 196–201 (1974)

**Publisher's Note** Springer Nature remains neutral with regard to jurisdictional claims in published maps and institutional affiliations.